Vol 16 No 8, August 2007
1009-1963/2007/16(08)/2439-05
Chinese Physics
© 2007 Chin. Phys. Soc.
and IOP Publishing Ltd

2D hydrodynamic simulation of a line-focused plasma in Ni-like Ag x-ray laser research*

Zheng Wu-Di(郑无敌)[a)b))†] and Zhang Guo-Ping(张国平)[a)]

[a)] *Institute of Applied Physics and Computational Mathematics, Beijing* 100088, *China*

[b)] *Graduated School of China Academy of Engineering Physics, Beijing* 100088, *China*

(Received 23 October 2006; revised manuscript received 12 February 2007)

In most collisional schemes of x-ray laser (XRL) experiments, a bow-like intensity distribution of XRL is often observed, and it is generally ascribed to the two-dimensional hydrodynamic behaviour of expanding plasma. In order to better understand its essence in physics, a newly developed two-dimensional non-equilibrium radiation hydrodynamic code XRL2D is used to simulate a quasi-steady state Ni-like Ag XRL experiment on ShenGuang-II facility. The simulation results show that the bow-like distribution of Ni-like ions caused by over-ionization in the central area of plasma is responsible for the bow-like shape of the XRL intensity distribution observed.

Keywords: x-ray laser, numerical simulation, line-focused plasma
PACC: 4255V, 5265

1. Introduction

In the research of x-ray laser (XRL) driven by laser, the driving laser is usually focused into a narrow line of about 100μm in width on a target,[1−5] and because of its large aspect ratio it causes the plasma produced to have a two-dimensional expansion. The two-dimensional hydrodynamic behaviour of the expanding plasma can be displayed by the field image of XRL observed in experiments. Figure 1 shows the intensity distribution of the quasi-steady state (QSS) Ni-like Ag 13.9 nm XRL observed on ShenGuang II laser facility, where the XRL is produced by using a laser beam (1ω/100ps/100J) focused into a 100μm×1.8cm line focus to irradiate an Ag slab target, and achieves an intensity of $(4-6)\times10^{13}$ W/cm^2. The driving laser beam includes two pulses, with an energy ratio of pre-pulse to main-pulse being $3\%-5\%$, the main-pulse is delayed about 3 ns. The output field images of XRL shown in Fig.1 look like a bow, and a similar shape has been also observed in most of XRL experiments conducted on other facilities.[1−4]

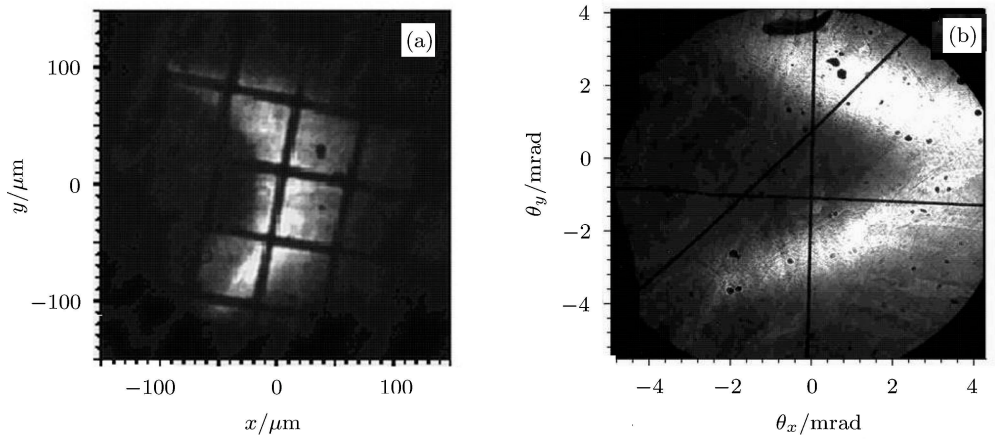


Fig.1. The intensity distribution of Ni-like Ag 13.9nm XRL, measured from experiments on ShenGuang-II facility. (a) Near-field image of two opposite coupling targets, in which the shadow grids are the supporting meshes on filter and the position of the initial target surface is not known for low radiation near the target. (b) Far-field image of single target with three fiducial wires, showing that the plasma expands rightward, with θ being the refractive angle.

*Project supported by the National High Technology Development Program of China (Grant No 803-804-7-1).
†E-mail: zheng_wudi@iapcm.ac.cn

There are two possible causes for this bow-like shape to occur. One is due to refraction; in other words, the XRL is refracted out of the central region because of a large electron density gradient. The other is that the gain spatial distribution of XRL might be of such a shape. In order to clarify these conjectures and to exactly understand the physical processes happening inside, a newly developed two-dimensional non-equilibrium radiation hydrodynamic code XRL2D is used to simulate the hydrodynamic behaviour of plasma under the same conditions as those in Fig.1. A brief introduction of the XRL2D code and the simulation results are presented in this paper.

2. Briefing of XRL2D code[6,7]

Inverse bremsstrahlung absorption and resonant absorption of driving laser are considered, and geometric optic approximation is used.[8] Flux-limit heat-conduction approximation and flux-limit multi-group diffusion approximation (about 100 groups) are adopted. The average atomic model only considering principal quantum numbers is used in the code. The micro-processes considered are bremsstrahlung, electron collisional ionization, photon ionization, electron collisional excitation, line emission, dielectronic recombination and their inverse processes.

In the view of Lagrange frame, the radiation hydrodynamic equations employed in the code are as follows:

$$\frac{\mathrm{d}\boldsymbol{u}}{\mathrm{d}t} = -\frac{1}{\rho}\nabla(p_\mathrm{e} + p_\mathrm{i} + p_\mathrm{r} + q), \tag{1}$$

$$\frac{\mathrm{d}(C_\mathrm{ve}T_\mathrm{e} + V)}{\mathrm{d}t} = -\frac{1}{\rho}\nabla\cdot\boldsymbol{F}_\mathrm{e} - p_\mathrm{e}\frac{\mathrm{d}}{\mathrm{d}t}\Big(\frac{1}{\rho}\Big) + W_\mathrm{ie} + W_\mathrm{l} - W_\mathrm{r}, \tag{2}$$

$$\frac{\mathrm{d}(C_\mathrm{vi}T_\mathrm{i})}{\mathrm{d}t} = -\frac{1}{\rho}\nabla\cdot\boldsymbol{F}_\mathrm{i} - p_\mathrm{i}\frac{\mathrm{d}}{\mathrm{d}t}\Big(\frac{1}{\rho}\Big) - W_\mathrm{ie}, \tag{3}$$

$$\frac{\partial f_\mathrm{v}}{\partial t} = -\nabla\cdot\boldsymbol{F}_\mathrm{r} + \frac{\rho\nu}{3}\frac{\partial f_\mathrm{v}}{\partial\nu}\frac{\partial}{\partial t}\Big(\frac{1}{\rho}\Big) + D_\mathrm{v} - C_\mathrm{v}f_\mathrm{v}. \tag{4}$$

Here, $\boldsymbol{u}$ is the hydrodynamic velocity, ρ is the matter density, p_e, p_i and p_r are respectively the electron pressure, ion pressure and radiation pressure, q is the von Neumann viscosity, $C_\mathrm{ve}T_\mathrm{e}$ and $C_\mathrm{vi}T_\mathrm{i}$ are the electron and ion internal energies per unit mass respectively, f_v is the photon number of unit quantum state, ν is the frequency of photon. V is the combining energy of ion, W_ie is the energy exchange between electron and ion, W_l is the deposited laser energy, W_r is the energy exchange between matter and radiation. D_v and C_v are the emission and absorption coefficients of photon, respectively. F_e, F_i and F_r are flux of electron, ion and radiation respectively.

$$\boldsymbol{F}_\mathrm{e} = \frac{\boldsymbol{F}_\mathrm{De}\cdot f_\mathrm{e}F_\mathrm{Le}}{|\boldsymbol{F}_\mathrm{De}| + f_\mathrm{e}F_\mathrm{Le}},$$

where f_e is the electron flux-limit factor, $\boldsymbol{F}_\mathrm{De}$ and $\boldsymbol{F}_\mathrm{Le}$ are the diffusion flux and direct flux respectively, $\mathrm{F}_\mathrm{De} = -K_\mathrm{e}\nabla T_\mathrm{e}$, $\boldsymbol{F}_\mathrm{Le} = N_\mathrm{e}kT_\mathrm{e}\sqrt{kT_\mathrm{e}/m_\mathrm{e}}$, and there are similar relations between the variables for ions and radiation correspondingly.

As the meshes can be severely distorted during the hydrodynamic calculation for the usual Lagrange method, the arbitrary-Lagrange-and-Euler (ALE)[9] method is adopted and it includes three steps. The first is the Lagrange step, in which the momentum equation is differentiated by using the integral gradient-average (IGA) scheme. And in order to reduce the calculation capacity, splitting scheme is used, that is, the diffusion processes of electron, ion and radiation are separated from local processes such as atomic processes, energy exchange between electron and ion, temperature rise induced by the deposited energy, and local photon-absorption and radiation, etc. As an implicit scheme is used, the local processes are all coupled with each other. For the diffusion equations, the nine-point scheme proposed by Kershaw[10,11] is used. The second step is to rezone meshes: the meshes are rezoned at each time-step in code. And the last step is remapping: a 2-order precision remapping scheme is adopted.[12]

3. Hydrodynamic simulation of QSS XRL

The calculation model is based on the experiment of Ni-like Ag XRL on ShenGuang-II in Fig.1. The thick Ag slab target is irradiated by two 100ps Gaussian pulses at 1.053 μm of wavelength, producing a 1.8 cm long and 100 μm wide focus line. The energies of the two pulses are 2.55J and 82.45 J separately, and the peak-to-peak delay time is about 3ns and the two pulses both are of flat-top shape in space. An electron flux-limit factor (f_e) of 0.03 is applied.

We consider the coordinate system shown in Fig.2, in which the driving beams irradiate the Ag slab target in the negative direction of the x-axis, and produce a plasma expanding in the opposite direction. In calculation, at the beginning, a physical region includes 30μm thick Ag target and an area filled with

low density Ag gas (a density of 10^{-6}g/cm^3) outside the target surface in the x-direction. And this physical region is divided into 150 meshes in the x-direction and 100 meshes in the y-direction. During calculation, meshes are kept perpendicular by re-zoning as shown in Figs.3 and 4. Owing to the symmetry of the problem considered here, only half physical area needs calculating.

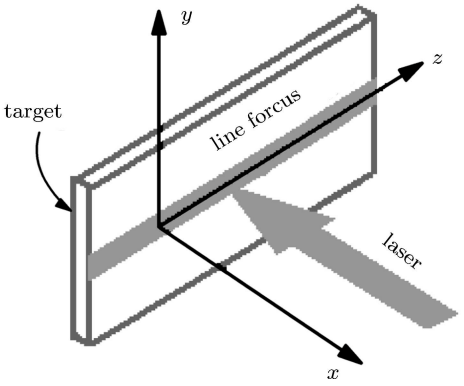


Fig.2. The geometry of the target irradiation, in which x and z are the directions of the driving laser and x-ray laser respectively.

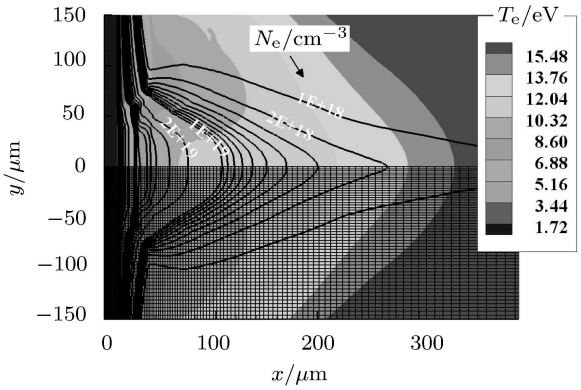


Fig.3. The electron temperature and density distribution before the main-pulse. Meshes are also plotted.

Figure 3 shows two-dimensional spatial distributions of the electron densities (in cm^{-3}) and electron temperatures (in eV) before the main-pulse, and the original target surface is located at the zero point of the horizontal axis with plasma expanding rightwards. Pre-pulse is used only to prepare a pre-plasma. After expanding for 3ns, the pre-plasma is cooled down to an electron temperature of no more than 20eV, while in the area near the target surface, the electron temperature decreases much more. Figure 4 shows the simulated results 20 ps after the peak time of the main pulse, when lasing of Ni-like Ag 13.9 nm XRL occurs (the result from 1D simulation of JB19 code[13−15]). It can be seen that the distribution of the abundance of the Ni-like ion is just a bow shape with an opening end facing the target surface. According to our simulation, within about 100 ps for the main pulse to irradiate the target, the plasma moves a little.

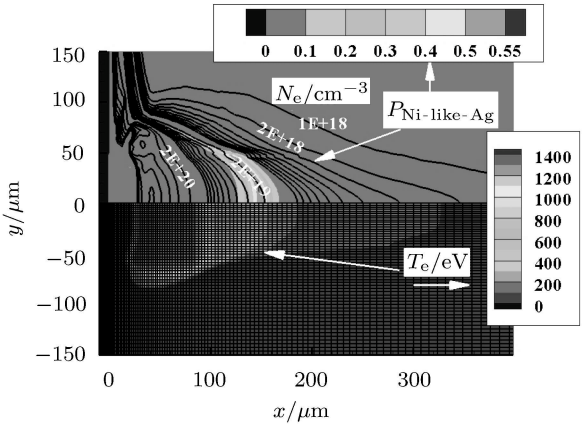


Fig.4. The electron temperature (in eV) and electron density (in cm^{-3}) distributions and fractional abundance of Ni-like ions 20ps after the main-pulse peak time.

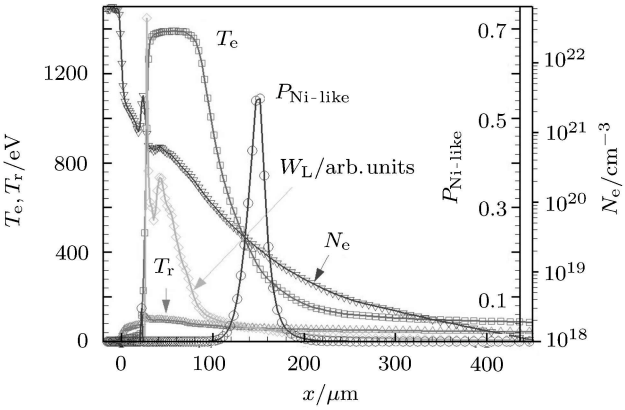


Fig.5. At the centre of the line focus, electron temperature T_e, radiation temperature T_r, electron density N_e, abundance of Ni-like ion $P_{\text{Ni-like}}$ and the deposited laser energy W_L, as functions of distance from the initial target surface, 20ps after main-pulse peak time.

With the arrival of the main-pulse, the plasma where the laser energy is deposited is heated and ionized dramatically through rapid electron collisional ionization. Thus the Ni-like ions are dominant at lower electron temperatures (< 300 eV). However, with the electron temperature further increasing, plasma becomes over-ionized quickly, so there is no more gain of Ni-like Ag XRL in this area. Through electron collision and radiation transfer, the energy

is transported out, then the plasma at lower densities (say, electron density $N_e = (1-4)\times10^{19}$ cm^{-3}) is warmed up. In this low-density area, the process of ionization is relatively slow, and a higher electron temperature ($T_e = 400-650$ eV) can be maintained when Ni-like ions are dominant, which can be seen in Fig.5. According to the experience of inversion kinetic calculation,[13−15] the gain can occur in this area about 150 μm away from the target surface.

Figure 6 shows the time evolution of the bow-like distribution of the Ni-like ions. And it can be seen that for the causes mentioned above, as time goes on, this bow-like shape moves slowly away from the target surface, and it gradually becomes bigger, and the two limbs become wider. Though the calculation of inversion kinetics has not been carried out, it can be predicted that the gain of the 13.9 nm XRL will distribute like a bow, too.

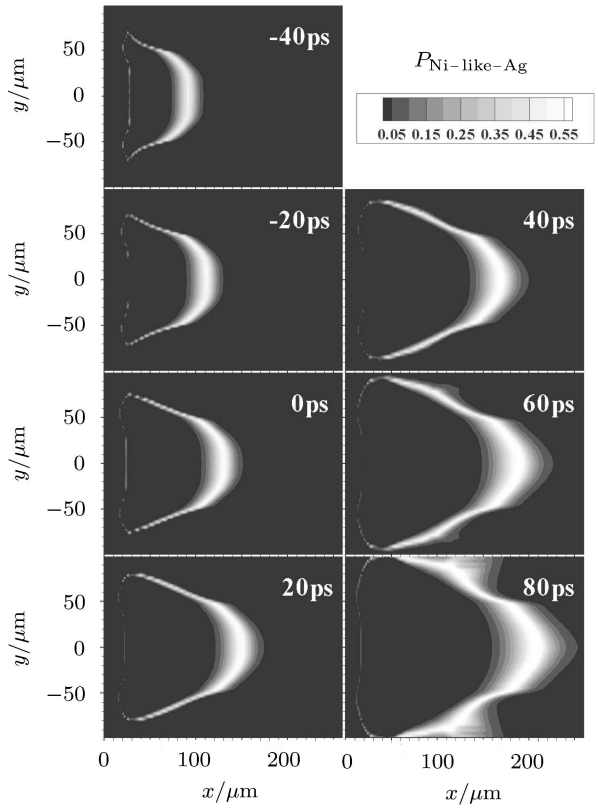


Fig.6. The time evolution of abundance distribution of Ni-like ions with the peak time of the main pulse being zero-valued

The gradient of electron density ($|\nabla N_e|$) is another important factor for intensity distribution of XRL. It can be seen from Fig.4 that the bow-like shape of Ni-like ion abundance has two narrow limbs, and gradient of electron density of the limbs ($|\nabla N_e| \sim 4.4\times10^{22}$cm^{-4}) is much larger than that in the central part ($|\nabla N_e| \sim 6.2\times10^{21}$cm^{-4}). According to the refraction law of XRL, for a long target (say, about 1cm long), the x-rays emitted from limbs cannot be amplified efficiently, so there are no thin and long limbs in near- or far-field intensity distribution of XRL. In addition, the refraction is not very serious for Ni-like Ag 13.9 nm XRL because of low electron density in the gain region ($< 10^{20}$ cm^{-3}) actually.

4. Conclusion

A bow-like distribution of Ni-like ion abundance is given by our simulation. The over- ionization occurs in a central area of plasma and it can induce the bow-like distribution of Ni-like ion abundance. This provides the evidence that the gain of QSS Ni-like Ag XRL has a bow-like distribution, which results in bow-like field images of XRL. The similar phenomena observed in Ne-like Ge and Ni-like Pd QSS XRLs may also be explained in the same way. As to the influence of refraction of XRL, the further calculations of inversion kinetics and propagation and amplification of XRL are needed.

The study of 2D effects of XRL is meaningful for better optimizing experimental conditions to obtain a high-intensity XRL, which is required to measure electron density and electron temperature of plasma.

References

[1] Zhang J, Warwick P J, Wolfrum E, Key M H, Danson C, Demir A, Healy S, Kalantar D H, Kim N S, Lewis C L S, Lin J, MacPhee A G, Neely D, Nilsen J, Pert G J, Smith R, Tallents G J and Wark J S 1996 *Phys. Rev.* A **54** R4653

[2] Nilsen J, Moreno J C, Luiz B, Da Silva L B and Barbee T W 1996 *Phys. Rev.* A **55** 827

[3] Nilsen J, Zhang J, MacPhee A G, Lin J, Barbee T W, Danson C, DaSilva L B, Key M H, Lewis C L S, Neely D, O'Rourke R M N, Pert G J, Smith R, Tallents G J, Wark J S and Wolfrum E 1997 *Phys. Rev.* A **56** 3161

[4] Siegel Ch, Braud M, Balmer J E and Nilsen J 2002 *Opt. Commun.* **210** 305

[5] Wang C, Wang W, Sun J R, Fang Z H, Wu J, Fu S Z, Ma W X, Gu Y, Wang S J, Zhang G P, Zheng W D, Zhang T X, Peng H M, Shao P, Yi K, Lin Z Q, Wang Z S, Wang H C, Zhou B, Chen L Y and Jin C S 2005 *Acta Phys. Sin.* **54** 202 (in Chinese)

[6] Chang T Q, Zhang J, Zhang J T, Lin D W, Lai D X, Shen L J, Xu L B and Chen G L 1991 *Laser–Plasma Interaction and Laser Fusion* (Hunan: Science and Technology Press)

[7] Li D Y, Xu G R, Shui H S, He G Y, Chen G N and Yuan G X 1987 *Two Dimensional Numerical Methods of Non-steady Hydrodynamics* (Science Press, printed in China)

[8] Duan Q S, Chang T Q, Zhang W Y, Wang G Y, Wang C J and Zhu S P 2002 *Chin. J. Comput. Phys.* **19** 57 (in Chinese)

[9] Hirt C W, Amsden A A and Cook J L 1974 *J. Comp. Phys.* **14** 227

[10] Kershaw D S 1981 *J. Comp. Phys.* **39** 375

[11] Duan Q S and Yuan G X 1997 *Chin. J. Comput. Phys.* **14** 148 (in Chinese)

[12] Benson D J 1992 *J. Comp. Phys.* **100** 143

[13] Zhang G P, Zhang T X and Zheng W D 2004 *High Power Laser and Particle Beams* **16** 1375 (in Chinese)

[14] Zhang G P, Zhang T X and Zheng W D 2005 *High Power Laser and Particle Beams* **17** 1817 (in Chinese)

[15] Zhang G P, Zhang T X and Zheng W D 2006 *High Power Laser and Particle Beams* **18** 210 (in Chinese)